Lab on a Chip

Devices and applications at the micro- and nanoscale

Accepted Manuscript

This article can be cited before page numbers have been issued, to do this please use: M. Rashidi, M. Nooryani, G. Natale and A. Benneker, *Lab Chip*, 2026, DOI: 10.1039/D5LC01020A.

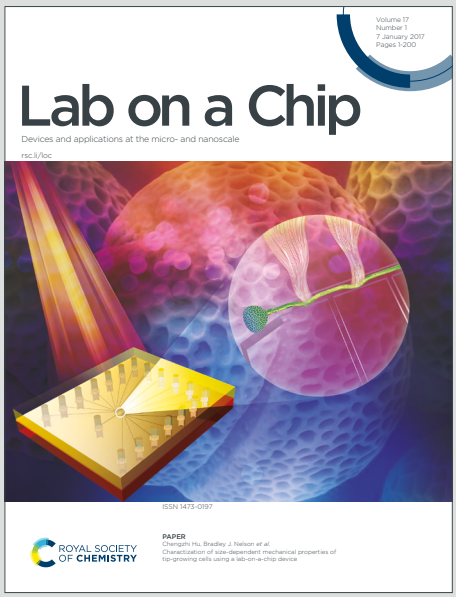

ROYAL SOCIETY OF CHEMISTRY

rsc.li/loc

View Article Online
DOI: 10.1039/D5LC01020A

Lab on a Chip

ARTICLE TYPE

Cite this: DOI: 00.0000/xxxxxxxxxx

Experimental Diffusiophoresis of Porous and Non-Porous Silica Particles in Dead-End Pore Microchannel Geometry

Mansoureh Rashidi[a], Matina Nooryani[a], Giovanniantonio Natale[a‡] and Anne M. Benneker[a‡]

Received Date
Accepted Date

DOI: 00.0000/xxxxxxxxxx

The movement of colloids in response to a concentration gradient of solutes, known as diffusiophoresis (DP), plays a crucial role in various applications, including separations, sorting and reactant transport. In this study, we experimentally investigate DP of porous and non-porous silica particles in different electrolyte solutions using a microfluidic system with a dead-end pore geometry. results are linked to a theoretical analysis, which reveals that the direction of particle motion is governed by the interplay between electrophoresis (EP) and chemiphoresis (CP), influenced by effects such as double layer polarization (DLP) and electroosmotic flow (EOF). The type of electrolyte has a significant impact on the overall behavior, as different ions have significantly different interactions with the particles and each other. The findings provide valuable insights into the DP behavior of porous particles, which can be leveraged to optimize particle transport in biomedical and environmental applications.

1 Introduction and Background

Diffusiophoresis (DP) is the movement of colloidal particles driven by a solute concentration gradient. In drug delivery, DP helps direct nanoparticles to specific target sites, increasing treatment efficiency and accuracy[1,2]. In microfluidics, it allows for precise manipulation and sorting of particles, which is crucial for the development of lab-on-a-chip devices[3,4]. DP was initially observed in non-electrolytes by Derjaguin et al. in the 1940s, and then was expanded to include electrolytes in the 1980s[5,6]. DP in non-electrolyte systems arises from particle-solute interactions within a diffuse interfacial layer surrounding the particles. These interactions, whether repulsive or attractive, create an osmotic pressure gradient along the particle surface as a result of local solute concentration differences. The osmotic pressure imbalance across the particle surface drives a flow, known as chemiosmosis (CO). This flow exerts a net force on the particle, causing chemiphoresis (CP) toward higher or lower solute concentrations, depending on whether interactions are attractive or repulsive[7–9]. In electrolyte solutions, there is an additional contribution to DP; electrophoresis (EP) resulting from an induced electric field[10]. EP (in DP) is driven by the electric field induced by the electrolyte concentration gradient, which arises because of differences in the ionic diffusivities of the solute. Initially, ions with higher diffusivity migrate faster, but Coulomb repulsion balances their migration rates, maintaining local electroneutrality within the solution[6,11]. The ratio of cation (D_+) and anion (D_-) diffusivities is described by the diffusion potential (β) defined as $\beta = \frac{D_+ - D_-}{D_+ + D_-}$ [12], and indicates the direction of the developed electric field. CP in electrolyte systems results from localized double-layer polarization (DLP) caused by the concentration gradient around the particle surface[10]. An electric double layer (EDL) with a thickness (λ) that is dependent on the local electrolyte concentration arises at the charged particle, where lower electrolyte concentrations result in larger EDLs. In a concentration gradient, the EDL thickness will change along the particle, and osmotic pressure differences will arise.

DP of non-porous particles has been extensively studied through theoretical[13,14], numerical[15,16], and experimental approaches[17,18]. In the literature, the DP velocity of a non-porous particle in a Newtonian fluid is defined as:

$$U_{DP} = \mu_{DP} \nabla \ln C(x,t) \tag{1}$$

In this equation, $C(x,t)$ is the solute concentration as a function of time and location in the system and μ_{DP} is the DP mobility of non-porous particles. For the case of a thin EDL ($\lambda \leq$ particle's radius), and a symmetric electrolyte, μ_{DP} can be defined as described in equation 2, where the first term represents the EP contribution, while the second term represents the CP contribution[19].

$$\mu_{DP} = \frac{\varepsilon k_B T}{\eta Z e} \left[\beta \zeta_p + \frac{4 k_B T}{Z e} \ln \left(\cosh \left(\frac{Z e \zeta_p}{4 k_B T} \right) \right) \right] \tag{2}$$

In this equation k_B is the Boltzmann's constant ($\frac{J}{K}$), T is the ab-

[a] Department of Chemical and Petroleum Engineering, Schulich School of Engineering, University of Calgary, AB, T2N 1N4, Canada

† Electronic Supplementary Information (ESI) available: [details of any supplementary information available should be included here]. See DOI: 10.1039/cXsm00000x/

‡ Corresponding authors: gnatale@ucalgary.ca, anne.benneker@ucalgary.ca

View Article Online
DOI: 10.1039/D5LC01020A

solute temperature (K), ε is the permittivity of the solution ($\frac{F}{m}$), e denotes the electron charge (C), Z is the ionic valence of the electrolyte's ionic species, η is the viscosity of the solution ($\frac{kg}{m.s}$) and ζ_p is the electrical surface potential (mV) of the particle which is the electric potential at the slipping plane between the Stern layer and the diffuse layer in the EDL[20].

DP of porous particles has been examined only through a limited number of theoretical and numerical studies[21–23]. Theoretical work derived the DP velocity of porous particles (presented in eq.3)[21], while numerical studies have investigated the impact of different parameters such as EDL thickness, surface charges, diffusion potential (β) of different electrolytes, and porosity on DP velocity of porous particles[21,22,24].

$$U_{DP} = \frac{\varepsilon|\nabla C|}{\eta C_0}\left(\frac{k_B T}{Ze}\right)^2[(\kappa a)^2\beta H_1\overline{Q} + (\kappa a)^4 H_2\overline{Q}^2 + O(\overline{Q}^3)] \quad (3)$$

In equation 3, κ is the inverse of the Debye length ($\lambda = \kappa^{-1}$) ($\frac{1}{m}$)[25], $\overline{Q} = \frac{ZeQ}{\varepsilon\kappa^2 k_B T}$ is the dimensionless fixed charge density of the porous particle. The first and second terms in eq.3 represent the EP and CP contributions to the DP motion of the porous particle, respectively. The terms H_1 and H_2 are functions of porous particle's permeability, EDL thickness, and the diffusion coefficient of the ionic species both outside and inside the porous particle[21]. The last term represents the equilibrium solution for the linearized Poisson–Boltzmann equation, which is applicable for small electric potential values (the Debye–Hückel approximation)[21]. From the available numerical and theoretical work, porous particles are expected to migrate faster than non-porous particles because (1) the interconnected pores in porous particles reduce the overall hydrodynamic drag force when compared to non-porous particles and (2) the fixed charges on the surface, distributed throughout the interior pore area, create a larger electric driving force that attracts more counter-ions into the particle interior, influencing the nominal charge of porous particles[26–28]. To the best of our knowledge, there are no experimental studies on how porous particles respond to an electrolyte concentration gradient. In this research, we investigate the behavior of porous particles with two different pore sizes under the influence of a temporary concentration gradient of various electrolytes and compare them with non-porous particles, using three different electrolyte compositions that have different values for β and pH.

2 Experimental Methods

2.1 Experimental Setup and Sample Preparation

Non-porous and porous particles are analyzed under an imposed concentration gradient using different electrolytes (HCl, NaOH and NaCl) in a microfluidic dead-end pore geometry, as used prior[29]. Figure 1 illustrates a schematic of the chip, consisting of two sections; (1) the main channel with width 300 μm and height 90 μm and (2) pores of 1000 μm long, 50 μm wide and 30 μm in height. This narrow, long pore geometry allows us to neglect the pressure gradient in y-direction across a single pore[30]. The height of the dead-end pores is thinner than that of the main channel to minimize disturbances from the main channel flow within the pores[31]. Consequently, this design can be considered to exhibit one-dimensional motion of colloidal particles in the x-direction under the influence of a transient concentration gradient, while external effects as a result of the flow in the main channel are minimized. Chips were fabricated by mixing PDMS and a curing agent (SYLGARD 184) in a 10:1 weight ratio, then pouring the mixture onto a silicon wafer mold (DRIE etched at Nanofab Co, Edmonton Alberta). After curing, PDMS was bonded to a microscope glass slide (75 × 25 × 1 mm, VWR) using a plasma cleaner (HARRICK PLASMA, Ithaca, NY, USA). Chips were left overnight prior to use to minimize the impact of changes in PDMS surface properties after fabrication.

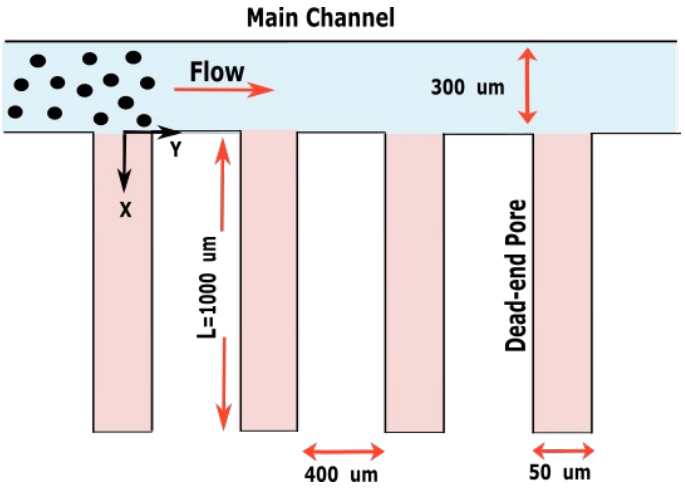

Fig. 1 Schematic of the microchannel with dead-end pore geometry used for diffusiophoresis (DP) experiments. Initially, the pores are filled with the corresponding electrolyte. Then, a suspension of particles in DI water is injected into the main channel. Upon reaching the pore entrances, the particles migrate either towards the higher or lower electrolyte concentration end, driven by the electrolyte concentration gradient.

Electrolyte solutions used in the experiments were prepared at a concentration of 10 mM, utilizing HCl (> 37% purity, Sigma Aldrich), NaOH (> 98% purity, Sigma Aldrich), and NaCl (> 99.5% purity, Sigma Aldrich). The experiments employed 1 μm non-porous silica particles and 1 μm porous silica particles (all SOLADTM particles, Glantreo) with two different pore sizes: 2 nm and 10 nm. Table 1 summarizes the characteristics of the porous particles used in this study. Silica particles were suspended in deionized (DI) water using a bath sonicator for 30 min at a concentration of 2.6×10^{-4} by volume, which is in the dilute regime to avoid particle-particle interactions. The EP mobility of silica particles (both non-porous and porous) was measured using a Dynamic Light Scattering instrument (Malvern Zetasizer Nano ZS) at various pH levels to observe EP mobility changes during DP experiments in different electrolyte concentration gradients. EP mobility (μ_{EP}) was measured instead of ζ-potential because, for porous particles, the validity of the Smoluchowski approximation at high ionic strengths ($\kappa a \geq 1$) is debated due to their distinct electrokinetic behavior compared to non-porous particles.

For each experiment, the 10 mM electrolyte solution was injected into the microfluidic channel using a syringe pump (Harvard Ap-

View Article Online
DOI: 10.1039/D5LC01020A

Table 1 Characterization of porous particles with 2 nm and 10 nm pore sizes, including BET surface area, pore volume, porosity, and tortuosity.

Property	Porous particle (2 nm pores)	Porous particle (10 nm pores)
BET ($\frac{cm^2}{gr}$)	624.60	196.24
Pore volume ($\frac{cm^3}{gr}$)	0.566	0.517
Porosity	36.8%	34.2%
Tortuosity	1.65	1.71

paratus, Pump 11 Elite). Once the main channel was filled, the outlet was blocked using a microfluidic valve to pressurize and fill the side channels. After ensuring that all channels were filled with electrolyte, the outlet blockage was removed and the injection of electrolyte continued for approximately 10-15 min to allow the system to reach equilibrium. Subsequently, the main channel was purged of electrolyte by introducing an air plug. The particle suspension was then injected into the main channel at a flow rate of 250 $\frac{\mu l}{h}$. Upon reaching the entrance of the first pore, the injection rate was reduced to 30 $\frac{\mu l}{h}$. Particle motion was observed using an optical microscope (ECHO, RVL-100-G) at a magnification of 20x, with images recorded at a frame rate of 8.3 frames per second. The motion of the particles under the influence of the electrolyte concentration gradient was recorded for approximately 600-700 s. All experiments were conducted at room temperature ($21 \pm 1^{\circ}C$). After recording particle motion in the presence of the electrolyte concentration gradient, ImageJ software (a Java-based image processing program)[32] was used to determine the maximum distance traveled by the particles within or away from the dead-end pores, denoted as L (μm). This value corresponds to the particle that reached the greatest distance from the pore entrance. The reported L values represent measurements obtained from two dead-end pores within the microchannel.

3 Results and Discussion

In electrolyte solutions, there are two types of double layer polarization leading to chemiphoresis[8,33]. The electrostatic attraction between the charged particle and counter-ions accumulated in the EDL on the higher-concentration generates a local electric field around the particle affecting particle motion. This type of polarization, called DLP type I, drives the particle towards the higher electrolyte concentration. DLP type II, is generated due to the electrostatic repulsive force between the charged particle and co-ions accumulated adjacent to the EDL. This creates another local electric field around the particle, driving it towards the lower electrolyte concentration[6,8,33]. Thus, the directions of these two induced electric fields are opposite to each other, as shown in Figure 2. Both the counter and co-ions move under the influence of these microscopic localized electric fields, resulting in electroosmotic flow (EOF) near the particle surface[8,34]. This EOF in turn contributes to the overall movement of the particles as a pressure gradient is induced. Depending on which DLP dominates, the movement as a result of CP can be in either direction.

To explain the observed behavior of particles in a temporary concentration gradients, it is important to consider that there is a higher ionic concentration near the particle on the side of higher electrolyte concentration. Consequently, the thickness of the EDL near that side of the particle is thin when compared to the lower concentration side, which is true for all our experimental configurations.

Here, we separately present the behavior of particles in three different electrolytes, the characteristics of which are described in Table 2. We define a positive direction of DP motion as particle movement towards the higher solute concentration (towards and into the dead-end pores) and a negative direction as particle movement towards the lower solute concentration (away from the dead-end pores). For all experiments, the effective diffusivity of the particles, expressed as $\frac{L^2}{t}$, is plotted for motion within the microfluidic chip in both directions (towards or away from the dead-end pores).

Table 2 Characterization of the electrolytes used in this study. D_+ and D_- represent the diffusion coefficients of the cation and anion, respectively, and β is the diffusion potential.

	HCl	NaOH	NaCl
D_+ ($\frac{m^2}{s}$)	9.31×10^{-9}	1.33×10^{-9}	1.33×10^{-9}
D_- ($\frac{m^2}{s}$)	2.032×10^{-9}	5.27×10^{-9}	2.032×10^{-9}
β	0.642	−0.596	−0.207

In the absence of a concentration gradient, particles penetrate only a short distance into the dead-end pore, approximately equal to the entrance length (L_e)[19]. L_e represents the distance from the pore inlet where the local velocity, typically reaches 99% of its fully developed value[35]. L_e is calculated using an empirical equation (eq. 4) applicable to rectangular cross-sections[36]. Here, Re is the Reynolds number defined as $\frac{\rho u w_{cs}}{\mu}$ for a rectangular channel, where w_{cs} is the width of the cross-section. Additionally, ρ and μ represent the fluid's density and viscosity, respectively. Since the electrolytes used in this study have density and viscosity values close to those of water, we used the properties of water at 20°C in our calculations. Specifically, we assumed $\mu = 1.0016$ mPa.S and $\rho = 998.2$ $\frac{kg}{m^3}$ to compute L_e, which was found to be 27.5 μm using eq. 4.

$$L_e = w_{cs}\left(\frac{0.55}{1+0.13Re} + 0.065Re\right) \quad (4)$$

3.1 Particles in HCl

Figure 3.A depicts the effective diffusivity of porous and non-porous particles under a temporary imposed HCl concentration gradient. When particles reach the inlet of the first dead-end pore, all different types of particles move into the pore towards the higher electrolyte concentration as shown in Figure 4. This indicates that CP dominates over EP, as schematically depicted in Figure 2A.

β is positive for HCl (see Table 2), which indicates that the background macroscopic electric field induced by the electrolyte concentration gradient, is directed towards the higher concentration of the electrolyte, as illustrated in Figure 2.A. Initially, the EP mobility (and thus ζ-potential) of the particles suspended in DI water pH = 7.14, is negative (Figure 7). With time, as the pH around the particles decreases, their absolute EP mobility decreases, but

View Article Online
DOI: 10.1039/D5LC01020A

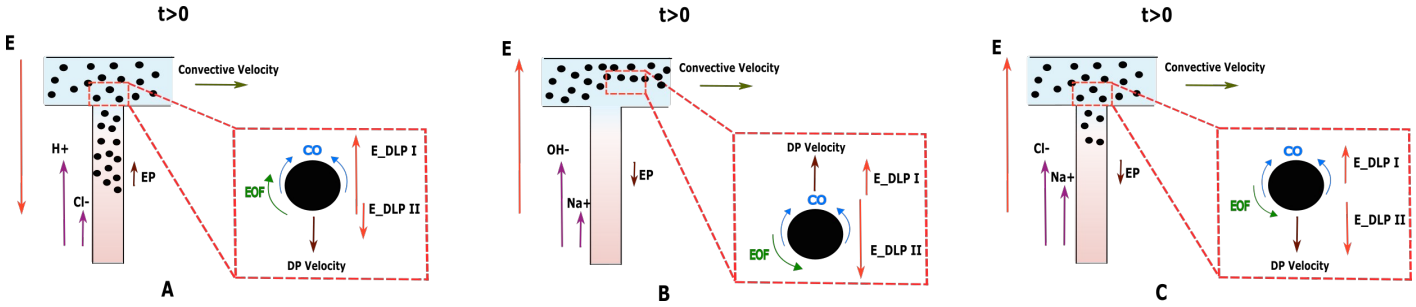

Fig. 2 Schematic representation of the mechanisms governing particle motion in different electrolytes during diffusiophoretic (DP) transport. A) In a HCl concentration gradient, both porous and non-porous silica particles migrate towards higher electrolyte concentration due to ion diffusion within the EDL (CO); and electroosmotic flow (EOF) aligning in the same direction overcoming the electrolphoresis (EP) under the influence of the background electric field. B) In a NaOH concentration gradient, porous particles move towards lower electrolyte concentration while non-porous particles move towards higher concentration. In this case, opposite directions of EOF and CO reverse the direction of solute diffusion on the particles' surface and consequently, the CP direction. For porous particles, the smaller absolute EP mobility, and the stronger influence of CP drives them toward lower electrolyte concentration. In contrast, for non-porous particles, the larger absolute EP mobility leads EP dominates CP, moving the particles towards higher electrolyte concentrations. C) In NaCl concentration gradient, both particle types migrate towards higher electrolyte concentration due to competing effects of two types of double layer polarization (DLP type I and DLP type II), along with the stronger influence of EP.

stays negative. In this case, as $\zeta\beta < 0$, EP is expected out of the channel in negative direction.

For HCl the faster diffusion of H^+ ions (in comparison to Cl^-) into the main channel and the attraction between the negatively charged particles and protons leads to their adsorption on the particle surface, reducing the effective surface charge of particles and subsequently lowering the absolute EP mobility. This results in a more pronounced establishment of DLP type I but a weaker DLP type II, consistent with previous reports[8,33]. Furthermore, as illustrated in Figure 2A, this DLP results in local EOF around the particles in the same direction as the developed chemi-osmosis (CO). This enhances the ion transport near the particles' surface and propels them toward the higher electrolyte concentration.

Overall, at low *p*H, as in the case of HCl, the particles exhibit a small absolute EP mobility, indicating a weakened EP response when compared to the CP response. This results in CP to dominate and drive both particle types toward the higher electrolyte concentration end.

Porous Particles

When porous particles reach the entrance of the dead-end pores, the attraction between the particles and positive ions such as H^+, along with penetration of these ions into the pores, significantly impacts their behavior. Calculations of κa, based on the concentration of H^+ ions, indicate a change from a maximum value of 330 in the pore to $\kappa a = 1$ when the electrolyte concentration gradient disappears and the electrolyte in the dead-end pores is approximated as DI water. At large κa, counter-ions can enter the pores of the particle, leading to partial or complete shielding of the particle's fixed charges. This phenomenon is referred to as the "counter-ion condensation" or "solidification" effect[1,11,37]. Therefore, at large κa, at the beginning of the experiments, the porous particles might become effectively charge-less. This charge neutralization is expected to suppress CP by reducing DLP on the outer surface which is the main driving force of CP in non-porous particles.

Figure 3.A shows that the effective diffusivity of porous particles is greater than that of non-porous particles. Such behavior indicates faster effective transport and is consistent with a higher DP velocity compared to non-porous particles. The DP motion of porous particles is generally faster than that of non-porous particles due to the more fixed charges distributed throughout the interior region of the particle, combined with the reduced hydrodynamic drag force[26–28] measured experimentally in this study (see Figure **??**, Appendix A). Particles with a pore size of 2 nm travel further into the dead-end pore compared to particles with a pore size of 10 nm. The "hindrance effect"[21,22] occurs when there is resistance to the diffusion of ions inside the porous particle. A smaller pore size can result in a more directed or focused movement of ions into the particle, leading to a stronger concentration gradient across the particle, and therefore, higher DP velocity[21,22]. The characterization data in Table 1 further support this idea; the smaller tortuosity value for the 2 nm pore particles suggests a less obstructed, more direct path for ion transport compared to the 10 nm pore particles, which directly contributes to their enhanced migration speed.

Numerical studies have shown that pore size, porosity and surface heterogeneity significantly influence the overall ζ-potential of porous particles[38,39], influencing their EP mobility. Particle heterogeneity causes deviations from traditional flat surface charge predictions seen in non-porous particles, where surface charge density decreases due to EDL overlap in the "valleys" and increases due to curvature effects on the "hills". The average ζ-potential and EP mobility is influenced by which effect is more dominant[39]. Additionally, the larger surface area and ion penetration into the pores of porous particles can enhance electrostatic screening, thereby reducing their effective surface potential. Consequently, the measured EP mobility of porous particles, which represents their ζ-potential, differs from that of non-porous particles within the same *p*H range, as shown in Figure 7. However, the measurements indicate that with reduced EDL overlap (at very low or very high *p*H), the EP mobility of porous and non-porous particles converges. Studies support that ion penetration,

View Article Online
DOI: 10.1039/D5LC01020A

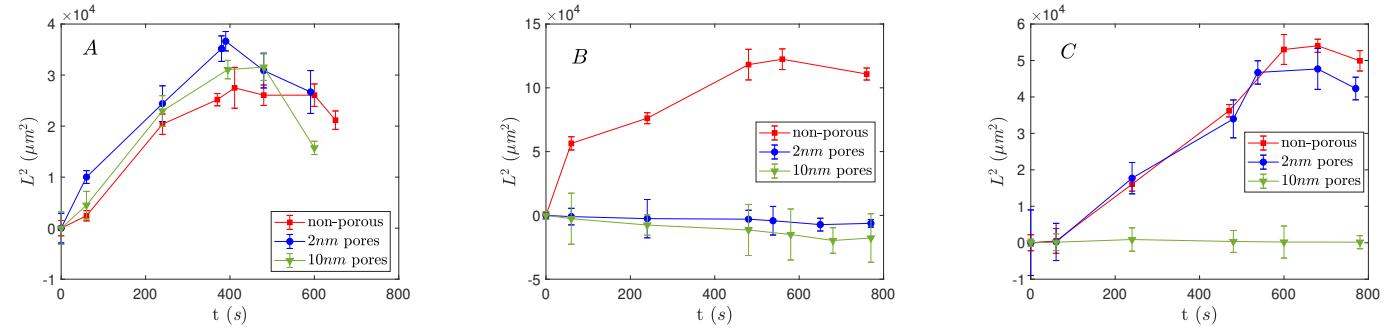

Fig. 3 Effective diffusivity of 1 μm non-porous silica particles and 1 μm porous silica particles with 2 and 10 nm pore sizes in dead-end pores under concentration gradient of different electrolytes over time: A) 10mM HCl electrolyte, B) 10mM NaOH electrolyte, C) 10mM NaCl electrolyte. Positive and negative L^2 indicate the direction of DP motion towards higher and lower electrolyte concentrations, respectively. Lines are to guide the eye.

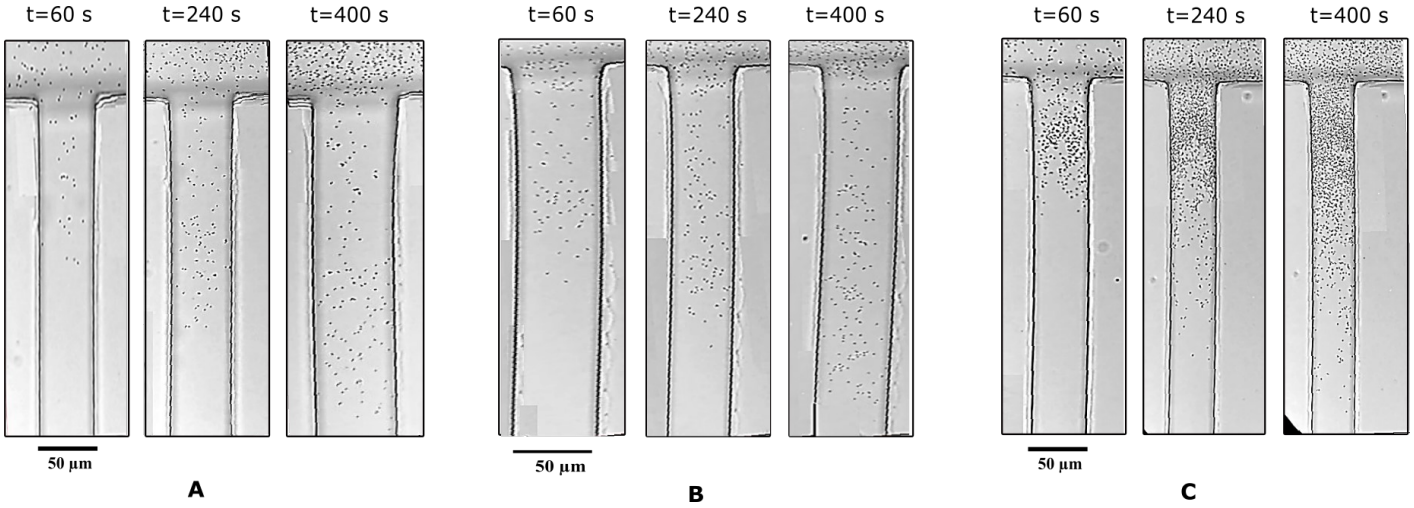

Fig. 4 DP motion of silica particles in microchannel with dead-end pore geometry under the influence of HCl concentration gradient as a function of time. A) non-porous particles, B) porous particles with 2 nm pore size, C) porous particles with 10 nm pore size

internal EDL overlap, and internal CP mechanisms can play an important role in porous particle transport[21,24]. In HCl solution, because counter-ion condensation reduces the effective surface charge, the strength of EP is weakened. CP therefore dominates, propelling porous particles toward regions of higher electrolyte concentration, in agreement with experimental observations.

Particle Movement Reversal

As our concentration gradient is transient, particle movement eventually slows down and reverses. According to the diffusivity of ions in the HCl electrolyte, the electrolyte concentration gradient in the dead-end pores is expected to disappear within 8.2 min. This time is calculated using $t = \frac{L^2}{D_i}$, where L is the length of the dead-end pore and D_i is the diffusivity of the electrolyte ions, based on the ion with the smaller diffusivity (Cl^-). As can be inferred from Figure 3.A, non-porous particles start leaving the dead-end pore (reduction of effective diffusivity) around 8.2 min, which corresponds closely to the calculated time for the disappearance of the electrolyte concentration gradient.

According to Figure **??**.A, the sequence of departure time for different particles under a temporary HCl concentration gradient is as follows: porous particles with 2 nm pore size leave first, followed by porous particles with 10 nm pore size, and finally, non-porous particles. We hypothesize that over time, the phenomenon of "counter-ion condensation" or "solidification" reduces the influence of CP, allowing EP to become the dominant mechanism driving the particles out of the dead-end pores[1,11,22]. This effect is more pronounced in porous particles due to ion diffusion into their internal structure, which accelerates the charge neutralization process and leads to earlier departure compared to non-porous particles. Furthermore, previous studies have shown that increased permeability; as in porous particles with 10 nm pores; slows the rate of charge neutralization or solidification[27]. This explains why 10 nm porous particles exit the channel later than those with 2 nm pores, despite both leaving earlier than their non-porous counterparts. Moreover, as the electrolyte within the dead-end pores is gradually replaced by DI water over time, the local *p*H increases. This rise in *p*H leads to an increase in the absolute value of the surface potential of the particles and consequently, their EP mobility (as shown in Figure 7), thereby enhancing the EP effect and further promoting particle migration out of the dead-end pores.

View Article Online
DOI: 10.1039/D5LC01020A

3.2 Particles in NaOH

Figure 3.B shows the effective diffusivity of particles under the concentration gradient of NaOH in the microchannel. Non-porous particles and porous particles with 2 and 10 nm pore sizes demonstrate distinct behavior, moving in different directions. In contrast to the case of HCl, in NaOH the anion moves faster and the local *p*H of both solutions are different, influencing the particles' EP mobility and ζ-potential.

The diffusion potential β is negative for NaOH (Table 2 indicates a background electric field towards the lower electrolyte concentration exists, as shown in Figure 2.B. The negatively charged particles are thus expected to move towards the higher electrolyte concentration due to EP (since $\zeta\beta > 0$). This is experimentally observed for non-porous particles (red squares).

As shown in Figure 7, EP mobility and consequently, surface potential remains negative across the *p*H range of $7-12$ for DI water and NaOH solution. As *p*H changes, the electrolyte concentration, EP mobility of the particles (representative of ζ-potential), and κa (or EDL thickness) also vary during the experiment. The absolute value of EP mobility for both particle types is greater in the NaOH solution compared to the HCl solution (Figure 7). When EP mobility is high, indicating a high particle surface potential, a strong repulsive force arises between particles and the co-ions (in this case, OH^-), which increases the amount of co-ions near the outer region of the high-concentration side of the EDL[6,15,33]. Due to the relatively slow diffusion of Na^+, lower concentration of counter-ions is present in the EDL at the top of the dead end channel, making DLP type II stronger than DLP type I. Therefore, co-ions have a greater influence on particle motion than counter-ions[8,28]. Due to the stronger induced electric field by DLP type II, an EOF in the opposite direction of the CO along the particle surface is created. This EOF could overcomes CO, reversing the ions diffusion direction within the EDL, and consequently, the CP direction, thereby driving particles toward the lower electrolyte concentration. This indicates that EP dominates over CP for non-porous particles in NaOH.

Porous Particles

In contradiction to solid particles, both types of porous particles move towards lower electrolyte concentrations under the same conditions, forming an exclusion zone at the entrance of the pores as depicted in Figure 5. Exclusion zones have been previously observed in microchannels with dead-end pore geometries[29]. When compared to non-porous particles, porous particles contain more fixed charges, which increase repulsion between co-ions and the negatively charged surface, leading to greater accumulation of co-ions near the EDL. This strengthens DLP type II in porous particles relative to non-porous ones, generating a stronger local EOF opposite to the direction of ion diffusion within the EDL (CO) and enhancing CP effects. The stronger EOF can potentially reverse the direction of ion diffusion within the EDL, thereby reversing the CP motion toward lower electrolyte concentrations. Additionally, the lower absolute EP mobility and therefore, ζ-potential of porous particles reduces the EP contribution. Together, these factors allow CP to dominate over EP in porous particles, driving them away from dead-end pores and toward the upper side wall of the main channel.

The exclusion zone thickness formed in the case of porous particles with a 2 nm pore size is smaller compared to those with a 10 nm pore size (smaller absolute magnitude of effective diffusivity in Figure 5). As a result, particles with 2 nm pores move less far away from the pores (see "hindrance effect" in Section 3.1).

Our observations reveal that the exclusion zone thickness decreases over time for both types of porous particles. Conversely, non-porous particles gradually exit the dead-end pores after a specific duration under the temporary NaOH concentration gradient, as depicted in Figure 3.B. The concentration gradient within the dead-end pores is expected to dissipate within 12.53min, calculated based the ion with the smaller diffusivity (Na^+). This suggests that the transient behavior observed for both porous and non-porous particles are likely influenced by the dissipation of the concentration gradient in the system, as was the case for HCl.

3.3 Particles in NaCl

The observation of DP motion of porous and non-porous particles in a temporary NaCl concentration gradient shows that porous particles with 10 nm pore size move to the the dead-end pores up to the entrance length described earlier. Non-porous particles and particles with small 2 nm pores, move into the dead-end pores (Figure 3.C and Figure 6). For NaCl, negative β (Table 2) creates a background electric field towards the lower electrolyte concentration as shown in Figure 2.C, similar to that of the NaOH case. As mentioned, the particles are initially negatively charged in DI water, and since $\zeta\beta > 0$, the background electric field drives negatively charged particles toward the higher electrolyte concentration.

Due to the higher diffusion rate of co-ions (D_{Cl^-}) and the repulsive force between the particles and co-ions, the resulting DLP type II is stronger than DLP type I, similarly to the NaOH case. Consequently, EOF in the opposite direction of CO forms along the particles surface. The close diffusivity magnitudes of Na^+ and Cl^- suggests that DLP type I and DLP type II compete, resulting in a weaker EOF along the particles surface compared to the NaOH case, where there is a larger difference in ion diffusivity. Although the EOF opposes the CO effect on the particle surface, it is not strong enough to reverse the direction of ion diffusion on the particle's surface. Therefore, the net effect of CP remains in the same direction as EP for particles in NaCl, and both mechanisms act cooperatively to drive particles toward the higher electrolyte concentration side. Since $\beta_{NaCl} < \beta_{NaOH}$, the background electric field and EP strength is weaker in NaCl compared to NaOH. This results in a smaller effective diffusivity into the dead-end pores under the imposed electrolyte concentration gradient, as shown in Figure 3.B and C.

Porous Particles

Compared to particles with 10 nm pores, Figure 6.A shows that those with 2 nm pores exhibit higher effective diffusivity and, consequently, higher DP velocity resulting in deeper penetration into the dead-end pores. This behavior is again attributed to the hindrance effect[22,40]. In contrast, particles with larger 10 nm pores experience greater fluid penetration and a stronger convection-

View Article Online
DOI: 10.1039/D5LC01020A

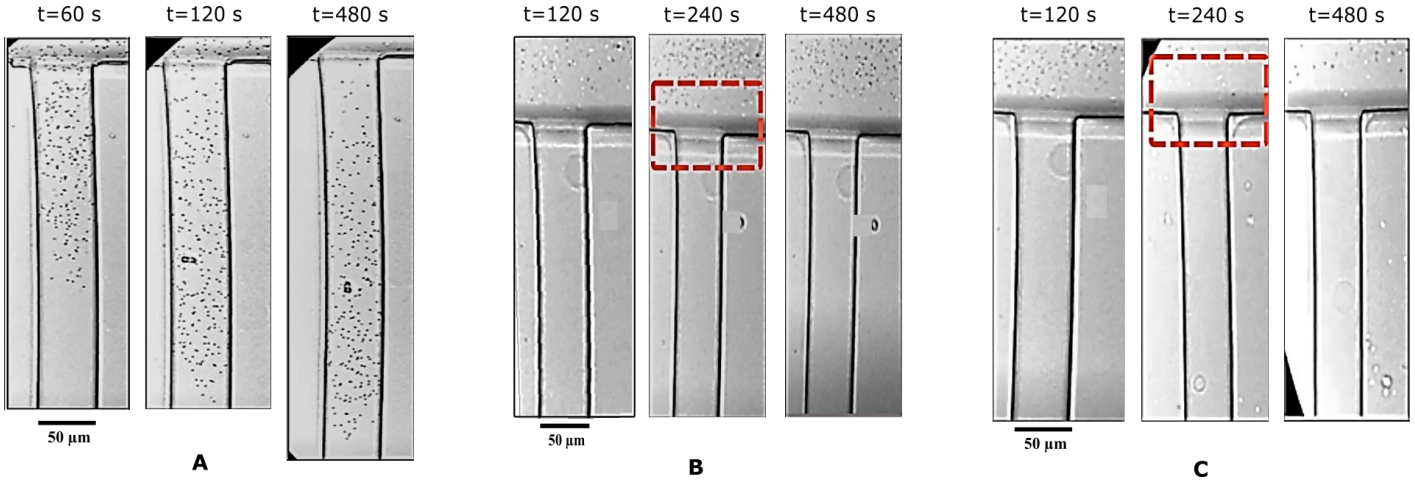

Fig. 5 DP motion of silica particles in microchannel with dead-end pore geometry under the influence of NaOH concentration gradient as a function of time. A) non-porous particles, B) porous particles with 2 nm pore size, C) porous particles with 10 nm pore size

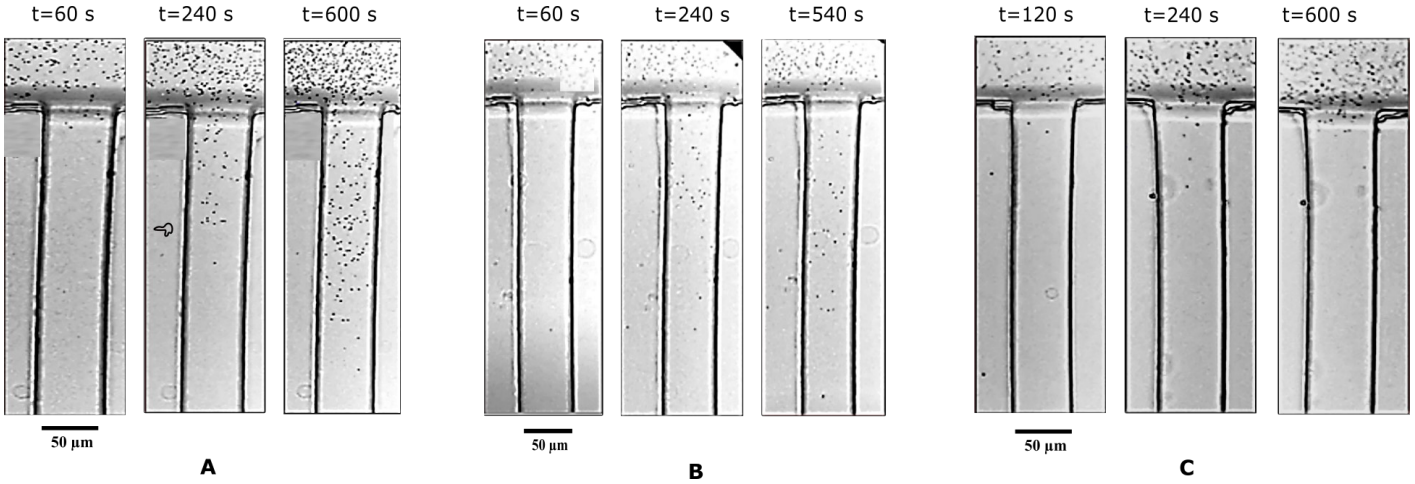

Fig. 6 DP motion of silica particles in microchannel with dead-end pore geometry under the influence of NaCl concentration gradient as a function of time. A) non-porous particles, B) porous particles with 2 nm pore size, C) porous particles with 10 nm pore size

induced motion-deterring effect, which reduces their DP velocity. Additionally, particles with 10 nm pores have the smallest absolute EP mobility ($\mu_{EP} = -1.14 \frac{\mu\text{m.cm}}{\text{v.s}}$), compared to particles with 2 nm pores ($\mu_{EP} = -1.74 \frac{\mu\text{m.cm}}{\text{v.s}}$) and non-porous particles ($\mu_{EP} = -2.05 \frac{\mu\text{m.cm}}{\text{v.s}}$). This implies weaker EP forces acting on them compared to NaOH case. Consequently, the combination of reduced EP and enhanced convective resistance acts to significantly reduce the effective DP velocity of these particles. As a result, their net migration into the dead-end pores is significantly restricted, with particles penetrating only up to the entrance length (L_e) based on the calculations in this study, as mentioned in section 3.

In experiments with non-porous and porous particles exposed to NaCl concentration gradient, both types of particles started to leave the dead-end pores as time progresses, similar to the behavior seen with HCl and NaOH. The concentration gradient within the dead-end pores is expected to dissipate within approximately 12.53 minutes, driven by the slower diffusion of Na^+ ions. This is linked to the dissipation of the concentration gradient within the system (Figure 3), as was the case in the other electrolytes.

3.4 Comparison to Theoretical Predictions

The velocity equations developed by Prieve et al.[6], shown in eqs. 5 and 6 are used to evaluate the relative significance of CP over EP. These equations are valid under the condition of $\kappa a \geq 1$ (small EDL thickness) and $\lambda e^{\frac{1}{2}|\overline{\zeta}|} \leq 1$. This allows the use of eq. 7 to estimate the velocity ratio of $\frac{U^{(c)}}{U^{(e)}}$, quantifying the contribution of CP relative to EP when particles are driven by a transient concentration gradient. In these expressions, γ is a dimensionless surface parameter defined as $\gamma = \tanh \frac{Ze\zeta}{4k_BT}$, $\overline{\zeta}$ is the dimensionless form of the ζ-potential, and C_∞ is the bulk concentration of electrolyte. To obtain the ζ-potential values used in these equations, the experimentally measured EP mobility (from DLS) was converted to ζ-potential using the Smoluchowski approximation.

In our system, generally, the required assumptions hold true, and calculated values of $\frac{U^{(c)}}{U^{(e)}}$ across a specific range of pH values that

View Article Online
DOI: 10.1039/D5LC01020A

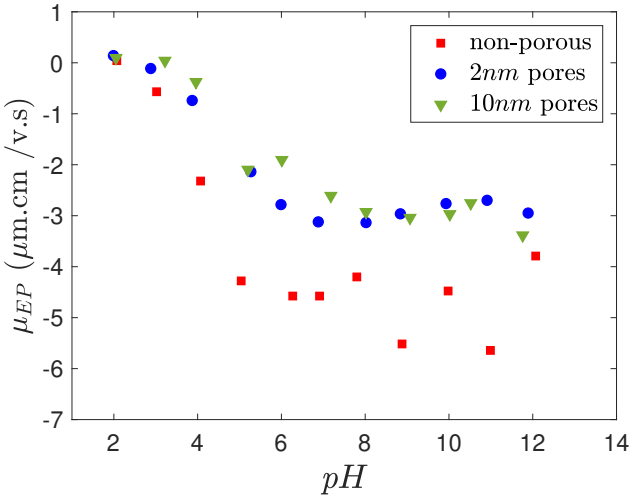

Fig. 7 EP mobility measurement of 1 μm non-porous silica particles and 1 μm porous silica particles with 2 and 10 nm pore sizes at different *p*H.

represent the potential *p*H variations under the different concentration gradients are summarized in Table 3. Empty cells in the table indicate *p*H conditions where the underlying assumptions are not valid and the velocity ratio cannot be reliably calculated.

$$U^{(c)} = \frac{\varepsilon}{2\pi\eta}\left(\frac{k_B T}{Ze}\right)^2[-\ln(1-\gamma^2)]\nabla \ln C_\infty \tag{5}$$

$$U^{(e)} = \frac{\varepsilon}{4\pi\eta}\left(\frac{k_B T}{Ze}\right)^2\beta\overline{\zeta}\nabla \ln C_\infty \tag{6}$$

$$\frac{U^{(c)}}{U^{(e)}} = \frac{-2\ln(1-\gamma^2)}{\beta\overline{\zeta}} \tag{7}$$

Table 3 Calculated velocity ratio of $\frac{U^{(c)}}{U^{(e)}}$ for non-porous particles and porous particles with 2 nm and 10 nm pore sizes under the transient HCl concentration gradient. The experiment captures particle behavior across the *p*H range of 2 to 7.

	$\frac{U^{(c)}}{U^{(e)}}$ non − porous	$\frac{U^{(c)}}{U^{(e)}}$ porous (2nm)	$\frac{U^{(c)}}{U^{(e)}}$ porous (10nm)
***p*H=2**	0.0046	0.0154	0.0105
***p*H=3**	−0.0619	−0.0121	0.0044
***p*H=4**	−0.2489	−0.0809	−0.0412
***p*H=5**	−0.4416	−0.2312	−0.2268
***p*H=6**	–	−0.2982	−0.2067
***p*H=7**	–	–	–

As shown, the absolute velocity ratio $\frac{U^{(c)}}{U^{(e)}}$ is smaller than 1 for all particles in the HCl system, indicating that in all cases EP velocity dominates over CP velocity, and this becomes more pronounced at lower *p*H. This is true for the gradients of NaOH and NaCl as well (see Table **??** and Table **??** in Appendix B). According to this, for HCl particles should migrate toward regions of lower electrolyte concentration, contradicting our experimental observations. For NaOH and NaCl these values indicate that particles are expected to migrate toward the region of higher electrolyte concentration. Only for NaCl, our experimental observations fully align with these estimations.

A possible explanation for these discrepancies is that in deriving the expressions for CP and EP, Prieve et al.[6] assumed a uniform electric field outside the EDL and did not account for microscale electric fields induced by ions accumulation around the particles. These local electric fields give rise to DLP type I and II, which significantly influence particles motion, especially for porous particles. Additionally, these expressions were derived for non-porous particles and are likely not valid for porous particles, where more complex phenomena can occur, such as ion penetration into the particle, formation and overlap of internal EDLs[38], and even potential EOF within the porous matrix can all affect particle motion[21]. Theoretical studies on DP velocity of porous particles[21] have shown that the DP transport of this type of particles should be treated as a volumetric phenomenon rather than a surface-driven one. When the fluid moves through the porous particle, it interacts directly with the fixed charge density distributed throughout the internal volume, rather than just a thin surface double layer. This means that the macroscopic EP and the CP, exert a force on every charged segment within the particle's interior. This internal coupling often causes the CP component to become more dominant. Consequently, the porosity and permeability of the particle do not just modify the velocity magnitude; they can fundamentally dictate the direction of motion by re-balancing the competition between the EP and the internal CP[21]. Another potential source of discrepancy for porous particles arises from the use of the Smoluchowski approximation to calculate the ζ-potential, which was used in estimating the ratio of CP to EP velocities. As mentioned earlier, the validity of this approximation for porous particles is not validated. Although in the theoretical model the effects of DLP type I and DLP type II are ignored, the close diffusivity of Na^+ and Cl^- likely leads to competing induced electric fields. This balance appears to validate the theoretical prediction in the NaCl case, in contrast to the electrolytes with large diffusivity differences.

To rule out the effect of *p*H variation in the channel on particle's motion in the system playing a dominant role, we numerically examined how changes in *p*H influence particle DP velocity. To analyze this process, the one-dimensional transient concentration gradient of H^+ was numerically solved using the equations presented in Appendix C[30,41]. As discussed previously, the long pore geometry allows the pressure gradient in the y-direction to be neglected[30] and the pores are designed to be thinner than the main channel to minimize disturbances from the main channel flow.

The results, shown in Figure 8 for HCl and Appendix C for NaOH, indicate that both non-porous and porous particles are predicted to have a negative velocity in HCl based on *p*H variations alone, while in the case of NaOH all types of particles are predicted to migrate toward the region of higher electrolyte concentration. Again, this is in contradiction to the experimental observations for most of the particles. Furthermore, the variation in *p*H does not induce a sign change of the particle ζ-potential, indicating that the particle movement reversal is not a result of the *p*H variation. Overall, this analysis of the effect of *p*H-variation cannot explain the experimentally observed particle behavior, supporting our hypothesis that the direction of particle motion is influenced

View Article Online
DOI: 10.1039/D5LC01020A

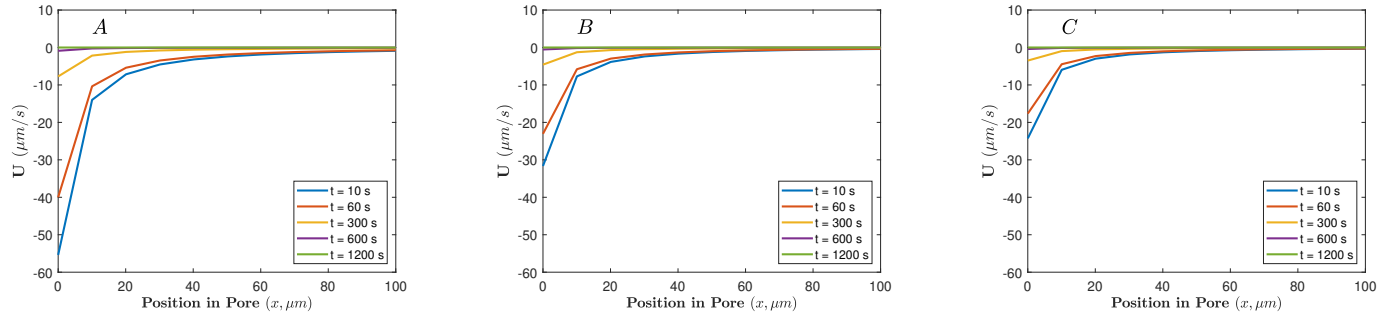

Fig. 8 Simulated DP velocity of particles in the microchannel over a 100 μm segment of the dead-end pore geometry under a transient concentration gradient of HCl as a function of time for A) Non-porous particles, B) porous particles with 2 nm pore size, C) porous particles with 10 nm pore size. In these plots, $x = 0$ represents the entrance of the dead-end pore, and $x = 1000\,\mu$m represents the end of the dead-end pore.

by the particle structure and the balance between EP and CP and is not dictated by the *p*H variation in the system.

4 Conclusions

In this experimental work, diffusiophoresis of porous and non-porous silica particles in dead-end microchannels under different electrolyte concentration gradients is investigated. The results show that electrolyte composition plays a key role in determining particle migration behavior, while the internal structure of porous particles further modifies their response. Overall, the study reveals a complex interplay between particle structure, interfacial electrokinetic phenomena, and electrolyte diffusivity.

In an acidic environment (HCl), where higher diffusivity of H^+ ions within the dead-end pores prevails, both porous and non-porous particles migrate towards regions of higher electrolyte concentration. Due to the attractive force between the negatively charged particle and H^+ ions, the DLP type I is stronger than DLP type II in this case. Consequently, the resulting EOF and the CO (diffusion of the ions on the particle surface) contributing to CP align, dominating over the weaker EP force, driving the particles towards the higher electrolyte concentration. Conversely, in a basic NaOH electrolyte, stronger DLP type II induces opposing EOF and CO contributions to CP, which can result in a reversal of the direction of the ionic diffusion flow on the particle's surface, thereby altering the CP direction toward the region of lower electrolyte concentration. Additionally, due to the smaller absolute value of the EP mobility of porous particles compared to non-porous particles, they are driven towards regions of lower electrolyte concentration, creating an exclusion zone at the entrance of the pores. In NaCl electrolyte, the close diffusivity of Cl^- and Na^+ ions result in the compensation of the two types of DLP. As a result, EP becomes dominant in driving both negatively charged porous and non-porous particles towards regions of higher electrolyte concentration. Notably, our study also highlights the significant reduction in drag forces experienced by porous silica particles compared to non-porous ones, a phenomenon influenced by pore size and permeability as confirmed through optical tweezers measurements.

To validate the experimental results, a theoretical velocity ratio of CP to EP was used to evaluate the relative contribution of each mechanism in driving particle motion. While the model successfully predicts particle behavior in the NaCl system, likely due to the balanced effects of DLP type I and type II, its predictions deviate from the experimental observations in the HCl and NaOH cases. This discrepancy is hypothesized to arise as the model does not account for microscale induced electric fields around the particle (associated with DLP type I and type II). In addition, it does not incorporate the complex dynamics involved in the DP of porous particles, such as ion penetration into the pores, overlap of internal EDLs, and EDL relaxation effects. The absence of these physical mechanisms limits the model's ability to accurately predict DP behavior in more complex systems. A numerical study was also conducted to examine the effect of *pH* variation in the system on the DP behavior of the particles. The results indicate that local *pH* variations do not alter the direction of motion of particles, further supporting the proposed mechanism and the physical interpretation of the observed DP behavior of porous particles.

Overall, our results demonstrate that DP transport in confined geometries such as dead-end pores is governed by both electrolyte properties and particle internal structure. There is a strong interplay between electrolyte composition and particle structure in determining both the direction and magnitude of particle migration. These findings provide practical design insights for microfluidic systems by showing that particle accumulation, exclusion, or penetration depth can be tuned through appropriate selection of electrolyte type and particle pore size. Such control over particle transport is relevant for applications including targeted particle delivery, sensing, passive separation, and controlled trapping of colloids in microfluidic and porous environments.

CONFLICT OF INTEREST

The authors declared no conflict of interest.

ACKNOWLEDGEMENTS

The authors acknowledge the financial support from Canada First Research Excellence Fund (CFREF).

View Article Online
DOI: 10.1039/D5LC01020A

Notes and references

1 O. Annunziata, D. Buzatu and J. G. Albright, *The Journal of Physical Chemistry B*, 2012, **116**, 12694–12705.

2 M. S. McAfee and O. Annunziata, *Langmuir*, 2015, **31**, 1353–1361.

3 S. V. Hartman, B. Božič and J. Derganc, *New biotechnology*, 2018, **47**, 60–66.

4 M. Seo, S. Park, D. Lee, H. Lee and S. J. Kim, *Lab on a Chip*, 2020, **20**, 4118–4127.

5 J. L. Anderson, *Annual review of fluid mechanics*, 1989, **21**, 61–99.

6 D. Prieve, J. Anderson, J. Ebel and M. Lowell, *Journal of Fluid Mechanics*, 1984, **148**, 247–269.

7 P. O. Staffeld and J. A. Quinn, *Journal of colloid and interface science*, 1989, **130**, 88–100.

8 J.-P. Hsu, W.-L. Hsu and Z.-S. Chen, *Langmuir*, 2009, **25**, 1772–1784.

9 J. Anderson, M. Lowell and D. Prieve, *Journal of Fluid Mechanics*, 1982, **117**, 107–121.

10 D. Velegol, A. Garg, R. Guha, A. Kar and M. Kumar, *Soft matter*, 2016, **12**, 4686–4703.

11 E. Lee, *Interface Science and Technology*, Elsevier, 2019, vol. 26, pp. 323–358.

12 T.-Y. Chiang and D. Velegol, *Journal of colloid and interface science*, 2014, **424**, 120–123.

13 H. J. Keh and Y. K. Wei, *Langmuir*, 2000, **16**, 5289–5294.

14 A. S. Khair, *Journal of Fluid Mechanics*, 2013, **731**, 64–94.

15 D. C. Prieve and R. Roman, *Journal of the Chemical Society, Faraday Transactions 2: Molecular and Chemical Physics*, 1987, **83**, 1287–1306.

16 S. Shim, M. Baskaran, E. H. Thai and H. A. Stone, *Lab on a Chip*, 2021, **21**, 3387–3400.

17 S. Shin, *Physics of Fluids*, 2020, **32**,.

18 S. Shim, J. K. Nunes, G. Chen and H. A. Stone, *Physical Review Fluids*, 2022, **7**, 110513.

19 S. Battat, J. T. Ault, S. Shin, S. Khodaparast and H. A. Stone, *Soft Matter*, 2019, **15**, 3879–3885.

20 D. Li, *Electrokinetics in microfluidics*, Elsevier, 2004.

21 Y. K. Wei and H. J. Keh, *Journal of colloid and interface science*, 2004, **269**, 240–250.

22 H. Y. Huang and H. J. Keh, *The Journal of Physical Chemistry B*, 2015, **119**, 2040–2050.

23 S. Marbach, H. Yoshida and L. Bocquet, *Journal of fluid mechanics*, 2020, **892**, A6.

24 S.-C. Tsai and E. Lee, *Langmuir*, 2019, **35**, 3143–3155.

25 M. v. Smoluchowski, *Band II, Barth-Verlag, Leipzig*, 1921, 366–427.

26 R. Wu and D. Lee, *Chemical Engineering Science*, 1998, **53**, 3571–3578.

27 P. P. Gopmandal, S. Bhattacharyya and B. Barman, *The European Physical Journal E*, 2014, **37**, 1–12.

28 E. Lee, *Interface Science and Technology*, Elsevier, 2019, vol. 26, pp. 385–409.

29 M. Nooryani, A. M. Benneker and G. Natale, *Lab on a Chip*, 2023, **23**, 2122–2130.

30 B. M. Alessio, S. Shim, E. Mintah, A. Gupta and H. A. Stone, *Physical Review Fluids*, 2021, **6**, 054201.

31 S. Shin, E. Um, B. Sabass, J. T. Ault, M. Rahimi, P. B. Warren and H. A. Stone, *Proceedings of the National Academy of Sciences*, 2016, **113**, 257–261.

32 J. Schindelin, C. T. Rueden, M. C. Hiner and K. W. Eliceiri, *Molecular reproduction and development*, 2015, **82**, 518–529.

33 Y. Pawar, Y. E. Solomentsev and J. L. Anderson, *Journal of colloid and interface science*, 1993, **155**, 488–498.

34 H. J. Keh and H. C. Ma, *Langmuir*, 2005, **21**, 5461–5467.

35 R. Shah, *Ducts, Supp. 1 of Advances in Heat Transfer*, 1978, 153–195.

36 T. Ahmad and I. Hassan, *Journal of Fluids Engineering*, 2010.

37 L.-H. Yeh and J.-P. Hsu, *Soft Matter*, 2011, **7**, 396–411.

38 F. E. Yakin, M. Barisik and T. Sen, *The Journal of Physical Chemistry C*, 2020, **124**, 19579–19587.

39 B. O. Alan, M. Barisik and H. G. Ozcelik, *The Journal of Physical Chemistry C*, 2020, **124**, 7274–7286.

40 W. Fang and E. Lee, *Journal of colloid and interface science*, 2015, **459**, 273–283.

41 E. Coleman and A. Gupta, *Physical Review Fluids*, 2025, **10**, 103701.

View Article Online
DOI: 10.1039/D5LC01020A

The data supporting this article have been included as part of the Supplementary Information. Raw data and additional information can be obtained from the corresponding authors.